Kinetic Studies on the N(^{2}D, ^{2}P) + CH_4 and CD_4 Reactions: The Role of Nonadiabatic Transitions on Thermal Rate Constants

Toshiyuki Takayanagi* and Yuzuru Kurosaki

Advanced Science Research Center, Japan Atomic Energy Research Institute, Tokai-mura, Naka-gun, Ibaraki 319-1195, Japan

Kei Sato, Kazuaki Misawa, Yasuhide Kobayashi, and Shigeru Tsunashima

Department of Applied Physics, Tokyo Institute of Technology, Ookayama, Meguro-ku, Tokyo 152-8551, Japan

Received: August 6, 1998; In Final Form: November 9, 1998

Thermal rate constants for the N(^{2}D,^{2}P) + CH_4 (CD_4) reactions have been measured using a technique of pulse radiolysis−resonance absorption in the temperature range between 223 and 298 K. Activation energies determined from the temperature dependence were about 1.5 and 1.0 kcal/mol for the reactions of N(^{2}D) and N(^{2}P), respectively. The H/D kinetic isotope effects were about 1.8 and 1.6 for N(^{2}D) and N(^{2}P), respectively. The rate constants for N(^{2}P) + CH_4 were much smaller than those for N(^{2}D) by a factor of 40−60. Variational transition-state theory calculations of the rate constants for the N(^{2}D) + CH_4 (CD_4) insertion reaction have been carried out using the reaction path information obtained from ab initio molecular orbital calculations. The comparison between the calculated and experimental rate constants shows that multiple surface coefficients are larger than the statistical value, meaning that nonadiabatic transitions are important for the N(^{2}D) + CH_4 reaction.

1. Introduction

The reactions of atomic nitrogen in the electronic ground-state or excited state are very important in interstellar, combustion, and atmospheric chemistries. Although the reactivity of atomic nitrogen has extensively been studied using active nitrogen,[1,2] which is the mixture of ground and excited atomic and molecular nitrogen, it is quite recent that the detailed mechanisms and dynamics of reactions of N with various molecules have been understood. On the experimental side, Umemoto and co-workers[3] recently used a technique of two-photon photolysis of NO to produce N(^{2}D), which makes it possible to perform pump−probe experiments under single collision conditions. They have applied this technique to the N(^{2}D) + H_2, CH_4, C_2H_6, and C_3H_8 reactions.[4−6] Casavecchia and co-workers[7] have recently succeeded in producing intense supersonic beams of N(^{2}D) and have performed crossed molecular beam experiments for the N(^{2}D) + H_2, C_2H_2, and C_2H_4 reactions.[8,9] Also, our laboratory has reported temperature dependence of thermal rate constants for the N(^{2}D) + H_2 and C_2H_2 reactions and their isotopic variants.[10,11] On the theoretical side, we have carried out ab initio molecular orbital (MO) calculations on the potential energy surfaces for the N(^{2}D) + H_2, CH_4, C_2H_2, and C_2H_4 reactions in order to understand reaction mechanisms as well as possible product channels.[11−14]

In this paper we will present experimental results for temperature dependence of the rate constants for the reactions of N(^{2}D,^{2}P) with CH_4 using a technique of pulse radiolysis−resonance absorption. The rate constants previously reported for these reactions are only at room temperature.[15−17] As mentioned above, Umemoto and co-workers[5] have experimentally studied the N(^{2}D) + CH_4 reaction under single collision conditions and detected NH($^3\Sigma$) as a primary product of this reaction. From the vibrational and rotational distributions of NH, they suggested that N(^{2}D) inserts into a CH bond to produce an intermediate radical. We previously performed ab initio MO calculations in order to understand the detailed reaction mechanisms of N(^{2}D) + CH_4 and confirmed theoretically that N(^{2}D) inserts into the CH bond.[13] We also carried out conventional transition state theory (TST) calculations of the rate constants using ab initio saddle point properties and compared the resulting values to the value of the experimental rate constant at room temperature. However, we could not discuss the accuracy of the ab initio results in detail because the experimental data for temperature dependence of the rate constants were not available at that time. Here we will use a more accurate variational transition state theory (VTST) with the results of ab initio reaction path analyses and compare the calculated rate constants to the experimental ones. It is expected that we can discuss the accuracy of the ab initio MO results as well as approximations used in the VTST calculations in detail.

2. Experimental Section

We employed a method of pulse radiolysis−resonance absorption to determine the temperature dependence of the rate constant. The procedure was very similar to that used for the N(^{2}D,^{2}P) + H_2,[10] C_2H_2,[11] and other molecular reactions.[16] A mixture of N_2 and CH_4 (CD_4) in a stainless steel vessel was irradiated by a pulsed electron beam from a Febetron 706 apparatus (Hewlett-Packard) to produce N(^{2}D) and N(^{2}P). The time profile of the concentration of N(^{2}D) and N(^{2}P) was monitored using the absorption of atomic lines at 149 (2^2D-3^2P) and 174 nm (2^2D-3^2P), respectively. In the present experiments, optical densities less than 0.5 were always used for the measurement of the relative concentration of the N(^{2}D)

* Corresponding author. E-mail address: tako@popsvr.tokai.jaeri.go.jp.

10.1021/jp9833146 CCC: $18.00
Published on Web 01/14/1999

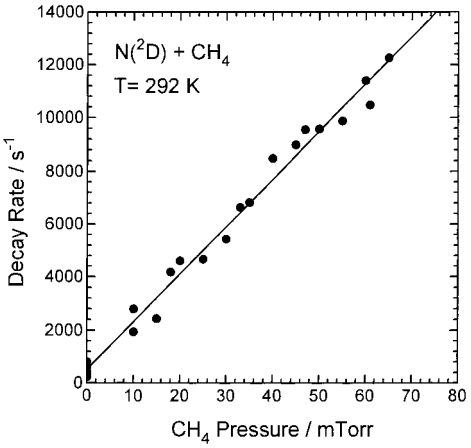

Figure 1. A typical plot of the pseudo-first-order decay rate of $N(^2D)$ as a function of CH_4 pressure at 292 K.

and $N(^2P)$ atoms so that Lambert−Beer's law approximately holds.[18,19] The atomic lines were derived from a CW microwave discharge in a flow of N_2/He. Transmitted light was detected with a photomultiplier tube (Hamamatsu, R976) through a VUV monochromator (Shimadzu, SGV-50). The signal was amplified and processed with a wave memory (NF Circuit Design Block, WM-852) and a personal computer (NEC, PC-9801RX). Since the spin−orbit fine structures of the atomic lines were not able to be resolved in the present experimental system, the rate constant obtained is averaged over spin−orbit sublevels. For the measurement of $N(^2P)$, the typical pressure of N_2 was kept at 700 Torr, while the CH_4 (CD_4) pressure was varied between 0 and 2.4 Torr. For the measurement of $N(^2D)$, the gas mixture was diluted with He because $N(^2D)$ is deactivated efficiently by N_2.[10] Typical pressures of CH_4 (CD_4), N_2, and He were 0−65 mTorr, 1 Torr, and 700 Torr, respectively. The initial concentration of the $N(^4S)$ atoms was previously estimated to be an order of 10^{13} molecule cm^{-3}.[19] Since the concentration of $N(^2D,^2P)$ is much smaller than that of $N(^4S)$ and that of CH_4 (CD_4), it can be postulated that the reaction is pseudo-first-order and the rate constants can be determined by measuring the decay rates of $N(^2D,^2P)$. CH_4 (purchased from Takachiho Shoji), CD_4 (ICON), N_2 (Taiyo-Toyo Sanso), and He (Union Helium) were used without further purification. The charging voltage of Febetron was varied in the range of 24−26 kV in order to check the effect of the radiolysis of CH_4 (CD_4) on the measured rate constant, but we found that the rate constant does not depend on the charging voltage.

3. Results and Discussion

A. Experimental Rate Constants. The time profile of the concentration of the $N(^2D)$ or $N(^2P)$ atom could be fitted with a single-exponential curve. This means that the concentration of the $N(^2D)$ or $N(^2P)$ atom decreases via the pseudo-first-order decay process, as mentioned previously. The decay rate was calculated by using a nonlinear least-squares fitting method. A typical plot of the decay rate as a function of the CH_4 pressure is shown in Figure 1. Each experimentally determined decay rate has an error of about 10%. The rate constant can be easily obtained from the slope of the linear plot. Table 1 summarizes the rate constants measured for $N(^2D) + CH_4$, $N(^2D) + CD_4$, $N(^2P) + CH_4$, and $N(^2P) + CD_4$; the error limit is two standard deviations. The rate constants are also compared to literature values in Table 1. The present result for $N(^2D) + CH_4$ at 292 K, $(5.4 \pm 0.3) \times 10^{-12}$ cm^3 $molecule^{-1}$ s^{-1}, overlaps the literature value of $(4.6 \pm 1.4) \times 10^{-12}$ cm^3 $molecule^{-1}$ s^{-1} at 300 K reported by Fell et al.[15] However, the present value is as 1.6 times as large as the literature value of $(3.33 \pm 0.22) \times 10^{-12}$ cm^3 $molecule^{-1}$ s^{-1} recently reported by Umemoto et al.[17] Also, the present value for $N(^2D) + CD_4$ at 298 K is larger than the value at 295 K measured by Umemoto et al. by a factor of 1.5. Umemoto et al.[17] employed a two-photon laser photolysis of NO to produce $N(^2D)$ and detected the $N(^2D)$ by monitoring the 149 nm fluorescence induced by the 269 nm two-photon excitation of $N(^2D)$, while Fell et al.[15] used a technique of electron spin resonance (ESR) absorption in a discharge flow system. The origin of these differences in the absolute value of the rate constants is unclear although our value of the H/D kinetic isotope effect is in good agreement with the value of Umemoto et al. (1.8 vs 1.7).

TABLE 1: Measured Rate Constants for the Reactions of $N(^2D)$ and $N(^2P)$ with CH_4 and CD_4

reaction	T/K	k/cm^3 $molecule^{-1}$ s^{-1}
present work		
$N(^2D) + CH_4$	292	$(5.4 \pm 0.3) \times 10^{-12}$
	273	$(4.0 \pm 0.3) \times 10^{-12}$
	253	$(3.6 \pm 0.2) \times 10^{-12}$
	233	$(2.8 \pm 0.2) \times 10^{-12}$
	223	$(2.3 \pm 0.2) \times 10^{-12}$
$N(^2D) + CD_4$	298	$(3.0 \pm 0.3) \times 10^{-12}$
	270	$(2.5 \pm 0.4) \times 10^{-12}$
	250	$(2.0 \pm 0.3) \times 10^{-12}$
	233	$(1.6 \pm 0.2) \times 10^{-12}$
	225	$(1.3 \pm 0.2) \times 10^{-12}$
$N(^2P) + CH_4$	292	$(9.3 \pm 0.6) \times 10^{-14}$
	273	$(8.4 \pm 1.0) \times 10^{-14}$
	253	$(6.6 \pm 0.7) \times 10^{-14}$
	233	$(6.1 \pm 0.8) \times 10^{-14}$
	223	$(5.7 \pm 0.6) \times 10^{-14}$
$N(^2P) + CD_4$	298	$(6.2 \pm 1.0) \times 10^{-14}$
	273	$(5.1 \pm 0.7) \times 10^{-14}$
	253	$(4.1 \pm 1.0) \times 10^{-14}$
	233	$(3.9 \pm 0.7) \times 10^{-14}$
	225	$(3.8 \pm 0.5) \times 10^{-14}$
literature values		
$N(^2D) + CH_4$	300	$(4.6 \pm 1.4) \times 10^{-12}$ [a]
$N(^2D) + CH_4$	295	$(3.33 \pm 0.22) \times 10^{-12}$ [b]
$N(^2D) + CD_4$	295	$(1.97 \pm 0.28) \times 10^{-12}$ [b]
$N(^2P) + CH_4$	295	$(7.7 \pm 0.5) \times 10^{-14}$ [c]

[a] Reference 15. [b] Reference 17. [c] Reference 16.

The temperature dependence of the measured rate constants is found to be well reproduced by the Arrhenius equation as shown in Figure 2; the Arrhenius parameters calculated by a nonlinear least-squares method are summarized in Table 2. Activation energies determined are almost the same (about 1.5 kcal/mol) for both the $N(^2D) + CH_4$ and $N(^2D) + CD_4$ reactions. Activation energies for the reactions of $N(^2P)$ are somewhat smaller than those for $N(^2D)$. From Tables 1 and 2, the values of the H/D kinetic isotope effects for $N(^2D)$ and $N(^2P)$ are about 1.8 and 1.6, respectively. It is interesting to note that the value for $N(^2D)$ is larger than the value predicted from the ratio of collision frequencies, i.e., the ratio of reduced masses. This suggests that the properties of the transition state are important for the reactions of $N(^2D)$ with CH_4 and CD_4. The present H/D kinetic isotope effects are also in contrast to the results of reactions with $H_2(D_2)$[10] or with $C_2H_2(C_2D_2)$.[11] In the case of $N(^2D,^2P) + H_2$ and D_2, the kinetic isotope effect was almost comparable to the ratio of collision frequencies.[10] In the case of $N(^2D,^2P) + C_2H_2$ and C_2D_2, the ratio of the measured rate constants was nearly unity and thus the kinetic isotope effect was nearly unity.[11]

It has been found that the rate constants for $N(^2P)$ are much smaller than those for $N(^2D)$ by a factor of 40−60. This means

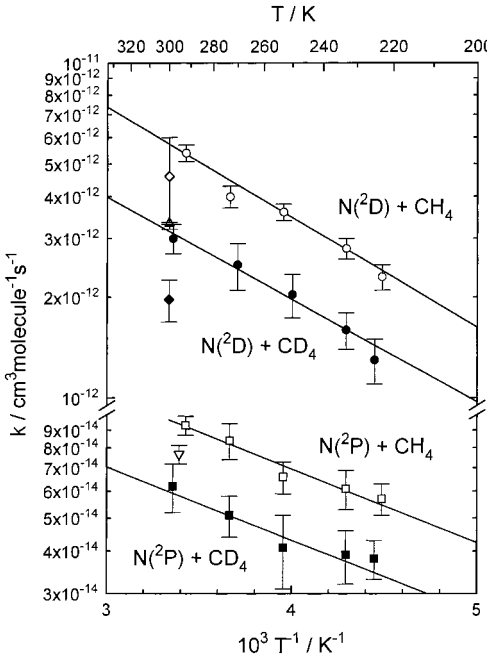

Figure 2. Arrhenius plots of the rate constants for N(^{2}D) + CH_4 (open circles), N(^{2}D) + CD_4 (solid circles), N(^{2}P) + CH_4(open squares), and N(^{2}P) + CD_4 (solid squares). The lines indicate Arrhenius fits to the corresponding experimental data. Literature values are also included: (◇) ref 15, (▽) ref 16, and (△ and ◆) ref 17.

TABLE 2: Arrhenius Parameters for the Reactions of N(^{2}D) and N(^{2}P) with CH_4 and CD_4

reaction	A/cm^3 molecule^{-1} s^{-1}	E_a/kcal mol^{-1}
N(^{2}D) + CH_4	$(7.1 \pm 4.4) \times 10^{-11}$	1.5 ± 0.3
N(^{2}D) + CD_4	$(3.3 \pm 1.4) \times 10^{-11}$	1.4 ± 0.1
N(^{2}P) + CH_4	$(5.0 \pm 2.2) \times 10^{-13}$	0.98 ± 0.22
N(^{2}P) + CD_4	$(3.1 \pm 1.4) \times 10^{-13}$	0.96 ± 0.24

that the N(^{2}P) atom is less reactive than N(^{2}D) despite that N(^{2}P) has higher electronic energy than N(^{2}D). Since small activation energies were observed for both the reactions, small rate constants for N(^{2}P) are mainly due to the small preexponential factor. This result is also similar to the reaction with H_2.[10] It has been reported that the rate constants for N(^{2}P) + H_2 are much smaller than those for N(^{2}D) + H_2 by a factor of 150−200 depending on temperatures.[10] The deactivation process of N(^{2}P) was previously discussed on the basis of adiabatic correlation between reactants and products by Donovan and Husain.[20] They proposed that the main exit channels may include physical deactivation processes to produce N(^{2}D) or N(^{4}S) because the N(^{2}P) + H_2 channel adiabatically correlates to the endothermic NH($A^3\Pi$) + H channel under C_s symmetry. Umemoto et al.[16] also suggested that the N(^{2}P) + CH_4 system may be very similar to the N(^{2}P) + H_2 case if the collision proceeds with C_s or C_{3v} symmetry. The reaction N(^{2}D) + CH_4 → NH($X^3\Sigma$) + CH_3 is exothermic by 26 kcal/mol.[13] The energy difference between N(^{2}D) and N(^{2}P) is 27 kcal/mol and the energy difference between NH($X^3\Sigma$) and NH($A^3\Pi$) is 85 kcal/mol.[20] Thus the reaction N(^{2}P) + CH_4 → NH($A^3\Pi$) + CH_3 is endothermic by 32 kcal/mol. Umemoto et al. then qualitatively concluded that the main deactivation process of N(^{2}P) by CH_4 is physical quenching to N(^{2}D) or N(^{4}S). However, further experimental studies including detection of primary products as well as theoretical studies of excited-state potential energy surfaces would be needed for understanding of the deactivation processes of the N(^{2}P) atom.

B. Variational Transition-State Theory Calculations. Compared to the deactivation processes of N(^{2}P), the reaction mechanism of N(^{2}D) + CH_4 is rather simple since previous experimental[5] and theoretical studies[13] reveal that the N(^{2}D) atom inserts into a CH bond in CH_4. The saddle point molecular structure obtained at the complete-active-space self-consistent-field (CASSCF) level was already reported in our previous paper.[13] As mentioned in the Introduction, we previously employed conventional TST; however, in this paper, we use more accurate VTST to calculate thermal rate constants. This is quite reasonable since the N(^{2}D) + CH_4 insertion reaction has a small classical barrier height and a loose saddle point structure, for which the variatonal effect is expected to be important.

In canonical VTST,[21] the position of the transition state along the reaction path is optimized at each temperature so as to minimize the calculated rate constant

$$k^{\mathrm{CVT}}(T) = \min k^{\mathrm{GT}}(T,s) \tag{1}$$

where

$$k^{\mathrm{GT}}(T,s) = f_e L \frac{k_B T}{h} \frac{Q^{\mathrm{GT}}(T,s)}{Q_r(T)} e^{-V(s)/k_B T} \tag{2}$$

Here $k^{GT}(T,s)$ is the generalized transition-state theory rate constant at the reaction path s.[21] k_B is the Boltzmann constant, h is Planck's constant, $Q_r(T)$ is the reactant's partition function, $Q^{GT}(T,s)$ is the partition function for the bound degrees of freedom orthogonal to the reaction path, and $V(s)$ is the value of the potential energy along the reaction path at s. L is the reaction path degeneracy (or statistical factor) and is 4 for the insertion reaction into a CH bond in CH_4. In the above expression, we explicitly use a "multiple surface coefficient", f_e,[22,23] which approximately takes the effect of electronic excited states into account. The multiple surface coefficient f_e, is generally given by the ratio of the number of reactive potential energy surfaces and the number of potential energy surfaces of reactants (or electronic degeneracy of reactants).[22] In the case of the N(^{2}D) + CH_4 reaction, if we assume that only the lowest doublet potential energy surface leads to reaction and the collision process proceeds adiabatically on this surface, we would have $f_e = 2/10 = 0.2$ since the electronic states of N(^{2}D) can be 10-fold degenerate with neglect of spin−orbit coupling. More precisely, the multiple surface coefficient with inclusion of spin−orbit coupling can be given by the ratio of electronic partition functions between transition state and reactants.[23] Again, if we assume the only the lowest doublet surface is reactive, f_e is given by $2/[6 + 4\exp(-\Delta E/RT)]$ for the N($^2D_{5/2,3/2}$) + CH_4 reaction, where ΔE (=8.7 cm^{-1}) is the spin−orbit splitting between N($^2D_{5/2}$) and N($^2D_{3/2}$). Thus, the values of f_e are calculated to be 0.203 and 0.205 at 300 and 200 K, respectively, which are comparable to the value calculated with neglect of spin−orbit coupling. This means that the spin−orbit coupling can be primarily ignored in the rate constant calculations for the N(^{2}D) + CH_4 reaction. However, it should be emphasized that $f_e \sim 0.2$ is obtained under the assumption that only the lowest doublet surface leads to reaction and that the collision process occurs only on this surface. Indeed, if all five doublet surfaces give reaction via nonadiabatic transitions, f_e would be nearly unity. This will be further discussed in detail below.

Quantum mechanical tunneling was not considered in the present VTST calculations, since our previous work[13] revealed that tunneling is less important for the N(^{2}D) + CH_4 reaction. This is mainly because the tunneling motion is associated with

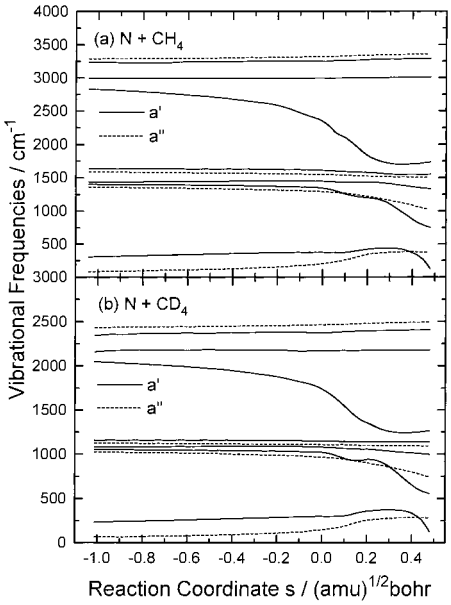

Figure 3. Harmonic vibrational frequencies as a function of the IRC path: (a) N(^{2}D) + CH_4 and (b) N(^{2}D) + CD_4. Solid and dashed lines correspond to a′ and a″ symmetry, respectively.

TABLE 3: Saddle Point Harmonic Vibrational Frequencies at the CASSCF(5,5)/6-311G Level**

symmetry	frequency/cm^{-1}
N(^{2}D) + CH_4	
a′	593i, 378, 1346, 1450, 1615, 2368, 2999, 3264
a″	203, 1294, 1551, 3322
N(^{2}D) + CD_4	
a′	504i, 305, 1024, 1085, 1149, 1744, 2179, 2386
a″	148, 968, 1109, 2465

the relative translational motion between N and CH_4, for which the corresponding reduced mass is relatively large.

All the information needed to calculate the VTST rate constants was obtained from ab initio MO electronic structure results. The intrinsic reaction coordinate (IRC) path for the N(^{2}D) + CH_4 insertion reaction was calculated at the CASSCF-(5,5)/6-311G** level of theory. The active orbitals were exactly the same as those used in our previous paper.[13] The harmonic vibrational frequencies along the IRC path were obtained from projected force constant matrices,[24] which were calculated at the same level of theory. These ab initio calculations were done using the Gaussian 94 programs.[25]

Figure 3 shows the vibrational frequencies along the IRC path for both the N(^{2}D) + CH_4 and N(^{2}D) + CD_4 reactions. Since the molecular geometries along the IRC path are within C_s symmetry, symmetry of each vibrational mode can be assigned as a′ or a″ as shown in Figure 3. Table 3 summarizes harmonic vibrational frequencies at the saddle point. The potential energies along the IRC path are plotted in Figure 4. The CASSCF energy profile is smooth and has a maximum of 2.8 kcal/mol. Also shown in Figure 4 are the vibrationally ground-state adiabatic potential curves (potential energy + zero-point energy) for both the N(^{2}D) + CH_4 and CD_4 reactions. It is interesting to note that the zero-point correction shifts the location of the potential maximum toward the reactants for both the reactions; the maximum occurs at $s = -0.21$ (amu)$^{1/2}$ bohr for CH_4 and at $s = -0.15$ (amu)$^{1/2}$ bohr for CD_4, respectively. This suggests that variational effects are rather important for these reactions.

The observed H/D kinetic isotope effect was found to be reproducible by the present VTST calculations. However, the absolute values of the VTST rate constants calculated using the

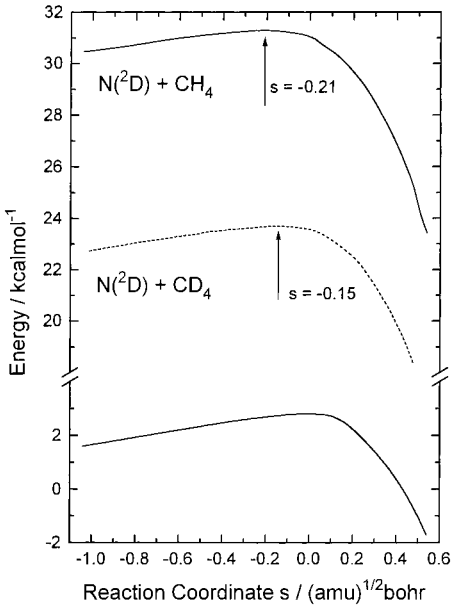

Figure 4. CASSCF potential energies (lower curve) along the IRC path and vibrationally ground-state adiabatic potential energies along the IRC path for N(^{2}D) + CH_4 (upper curve) and for N(^{2}D) + CD_4 (middle curve). Arrows indicate potential maxima.

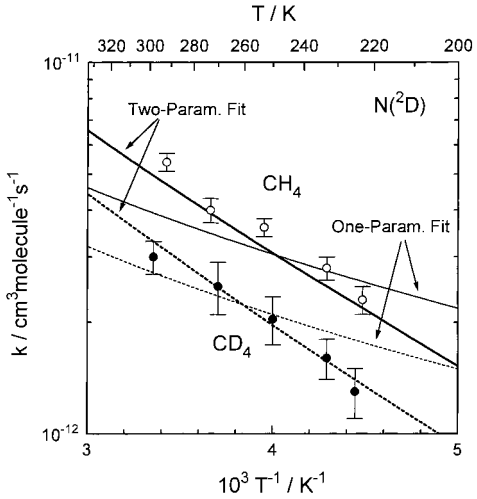

Figure 5. Arrhenius plots of the rate constants for the N(^{2}D) + CH_4 and CD_4 reactions. Lines represent the VTST rate constants. Open and solid circles correspond to the present experimental data.

ab initio potential surface information were much smaller than the experimental values. For example, the VTST rate constant at 292 K (with $f_e = 0.2$) is calculated to be 8.5×10^{-14} cm^3 molecule^{-1} s^{-1}, which is smaller than the experimental value at the same temperature by a factor of about 60. This serious disagreement is primarily attributed to the inaccuracy in the classical barrier height obtained at the CASSCF level calculations; the value of 2.8 kcal/mol is too large. Therefore, we adjusted the classical barrier height by multiplying a factor to the potential energy function along the IRC path: $V'(s) = \alpha V(s)$. The value of α was determined so as to reproduce the experimental data. The result of this fitting is shown in Figure 5, and the value of α was determined to be 0.17 ± 0.02. This indicates that the classical barrier height should be reduced to 0.47 kcal/mol so as to approximately reproduce the absolute values of the experimental rate constants. However, a significant deviation from the experimental temperature dependence can be seen in Figure 5. This means that it may be impossible to

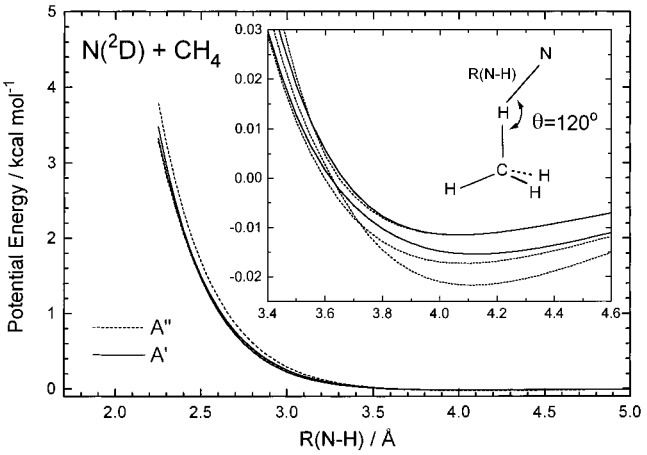

Figure 6. Ab initio potential energies for five doublet electronic states which asymptotically correlate to $N(^2D) + CH_4$ as a function of the internuclear distance between N and H. Solid and dashed lines are for A″ and A′ symmetry, respectively. An insert is an expansion of the potential energies in a van der Waals region.

reproduce the experimental data only by adjusting the barrier height.

Next, we treated the multiple surface coefficient f_e as an additional adjustable parameter. Therefore, two parameters, f_e and α, were determined so as to reproduce the experimental data by a nonlinear least-squares method. By adding f_e to fitting parameters, we were able to fit the VTST rate constants to the experimental data satisfactorily. The results are plotted in Figure 5. The value of α was determined to be 0.46 ± 0.10 with one standard deviation. This indicates that the barrier height is in the range of 1.0−1.6 kcal/mol. On the other hand, the value of f_e was calculated to be 0.95 ± 0.43 with one standard deviation. Since the condition with $f_e > 1$ is physically meaningless, the value of α is in the range of 0.52−1.0. Thus, it can be concluded that the multiple surface coefficient should be much larger than the value predicted from the electronic degeneracy (0.2) in order to explain the present experimental data; even the lower limit of the coefficient (0.52) is larger by a factor of 2.6. This result strongly suggests that nonadiabatic transitions are very efficient for the $N(^2D) + CH_4$ reactions.

To qualitatively understand the importance of nonadiabatic transitions, we calculated five doublet potential energy curves which asymptotically correlate to $N(^2D) + CH_4$ as a function of the internuclear distance between N and one of the H atoms in CH_4. The molecular geometry of CH_4 was kept in its equilibrium structure and only C_s symmetry was considered. The angle N−H−C was set to be 120°, which is comparable to the value of the saddle point structure. In this calculation, the second-order configuration interaction wave function, for which only three N2p orbitals were treated as valence orbitals, was employed with the triple-ζ + polarization basis set. Molecular orbitals were determined from the restricted open-shell Hartree−Fock method. This ab initio calculation was done using the HONDO7 program.[26] The calculated result is plotted in Figure 6. It can be seen that all five doublet states are asymptotically attractive and the five doublet potential energy curves have very shallow van der Waals wells. Also, it is interesting to note that these five doublet states are very close in energy and crossing or avoided crossing points can be seen in the range of 3.2−3.7 Å. This means that there may exist more avoided crossing points in this region when the molecular symmetry is reduced to C_1 symmetry from C_s symmetry. We have also carried out similar configuration interaction calculations for the transition-state geometry in order to understand the effect of the excited-state potentials at the transition state. We have found that the first excited state ($^2A'$) is 4.6 kcal/mol higher in energy than the lowest doublet state ($^2A''$). Other three doublet states were about 20 kcal/mol and more higher in energy than the lowest doublet state. This result indicates that only the lowest doublet potential energy surface leads to reaction under thermal condition and that nonadiabatic transitions are not important around the transition state region. Thus, it is suggested that nonadiabatic transitions play a significant role only in asymptotic region. The second-order configuration interaction method employed here is not very accurate enough for quantitative descriptions of potential energy surfaces since the effect of electron correlation in CH_4 is not fully taken into account. Nevertheless, the present experimental results can qualitatively be explained if the transition probabilities among the five doublet states would be large.

C. General Discussion on Multiple Surface Coefficients. The conventional approach to the inclusion of electronically excited states in the calculation of rate constants involves multiplying a rate constant calculated on the lowest electronically adiabatic potential energy surface by a "multiple surface coefficient"[22,23] which is defined as the ratio of transition state to reagent electronic partition functions,[23] as mentioned previously. This approximate approach is usually employed in the TST calculations, as has been done in a previous section. In the case of the $N(^2D) + CH_4$ reaction, the multiple surface coefficient should be 0.2 since the electronic state of $N(^2D)$ is 10-fold degenerate without a spin−orbit interaction. The present experimental results suggest, however, that this simple approximation cannot be applied to the reaction of $N(^2D)$ with methane and that nonadiabatic transitions play important roles in collision dynamics although the rate constant calculations have been carried out within a framework of VTST using ab initio reaction path information.

It may be generally difficult to discuss the validity of the "multiple surface coefficient" from a theoretical point of view since we have to employ a multiple surface quantum reactive scattering method. Schatz[27] has performed exact quantum scattering calculations including the effect of atomic fine structures for the $Cl(^2P_{3/2,1/2}) + HCl$ reaction and discussed the accuracy of the simple approximation with electronic partition functions mentioned above. As far as we are aware, this is only one report in which the accuracy of this approximation is quantitatively discussed. He has found that the approximation using the multiple surface coefficient is very accurate and that the Cl + HCl reaction is in the adiabatic limit with respect to the correlation between asymptotic and saddle point electronic states. However, the classical barrier height for this reaction (8.6 kcal/mol) is much larger than that for the $N(^2D) + CH_4$ reaction. Also, a simple LEPS potential energy surface, which does not include long-range van der Waals attractive interactions, was employed in the quantum scattering calculations of Schatz. In addition, the Cl + HCl reaction is a very simple atom + diatom reaction, and the dominant reaction path is collinear. On the other hand, $N(^2D) + CH_4$ is an atom + polyatomic molecule reaction and it is expected that molecular geometries with C_1 symmetry significantly contribute to the total reaction rate constants although the saddle point geometry for $N(^2D) + CH_4$ has C_s symmetry. Therefore, it may not be clear if the conclusion obtained from the quantum scattering calculations on the Cl + HCl reaction can be applicable to the $N(^2D) + CH_4$ reaction system.

Interestingly, Clary et al.[28] have found that nonadiabatic transitions play important roles in several ion−molecule reac-

tions. They found that experimental rate constants for 34 exothermic reactions of C^+ and N^+ ions with molecules are in the range between $f_e k_c$ and k_c, i.e., $f_e k_c < k_{exp} < k_c$, where k_{exp} denotes the experimental rate constant and k_c is the theoretical rate constant calculated with the adiabatic capture centrifugal sudden approximation. In addition, there are several reactions for which k_{exp} agrees with the upper limit k_c or the lower limit $f_e k_c$. They concluded that, in the former case, nonadiabatic transitions must be very efficient so that transfer from a potential surface to another surface occurs with unit probability. In the latter case, such nonadiabatic transitions are not important. Note that the interactions between ions with molecules are generally attractive and do not have any reaction barriers; however, these results are very similar to the present result.

Although further theoretical studies including extensive calculations of excited-state potential energy surfaces will definitely be necessary to discuss quantitatively the importance of nonadiabatic transitions, it should be emphasized that nonadiabatic transitions play a significant role from the comparison of the experimental rate constants for $N(^2D) + CH_4$ to the VTST rate constants with ab initio reaction path information. In addition, a simple approximate method or model to predict the contribution of nonadiabatic transitions to thermal rate constants should be developed in calculating TST rate constants in a future.

4. Conclusions

Thermal rate constants for $N(^2D,^2P) + CH_4(CD_4)$ have been measured using a technique of pulse radiolysis−resonance absorption between 223 and 298 K. Arrhenius parameters have been determined from the temperature dependence of the rate constants; activation energies for $N(^2D) + CH_4$ and CD_4 were about 1.5 kcal/mol while those for $N(^2P)$ were about 1 kcal/mol. The H/D kinetic isotope effects were about 1.8 for $N(^2D)$ and 1.6 for $N(^2P)$, respectively. The rate constants for the reactions of $N(^2P)$ were much smaller than those for $N(^2D)$ by a factor of 40−60. One of the deactivation processes of $N(^2P)$ is physical quenching to $N(^4S)$ or $N(^2D)$; however, the contribution of chemical reactions cannot be ruled out.

The canonical VTST calculations have been carried out for $N(^2D) + CH_4$ using ab initio reaction path information obtained at the CASSCF(5,5)/6-311G** level. The comparison between the calculated and experimental rate constants suggests that the classical barrier height for this reaction is about 1.3 kcal/mol and that a "multiple surface coefficient" is much larger than the statistical value (0.2) obtained from electronic degeneracy. This suggests that nonadiabatic transitions in asymptotic regions may play an important role in the collision dynamics between $N(^2D)$ and CH_4.

Acknowledgment. The authors thank Prof. Umemoto for a helpful discussion and supplying experimental data prior to publication.

References and Notes

(1) Brocklehurst, B.; Jennings, K. R. *Prog. React. Kinet.* **1967**, *4*, 1.
(2) Safrany, D. R. *Prog. React. Kinet.* **1971**, *6*, 1.
(3) Umemoto, H.; Matsumoto, K. *J. Chem. Soc., Faraday Trans*. **1996**, *92*, 1315.
(4) Umemoto, H.; Asai, T.; Kimura, Y. *J. Chem. Phys*. **1997**, *106*, 4985.
(5) Umemoto, H.; Kimura, Y.; Asai, T. *Chem. Phys. Lett*. **1997**, *264*, 215.
(6) Umemoto, H.; Kimura, Y.; Asai, T. *Bull. Chem. Soc. Jpn*. **1997**, *70*, 2951.
(7) Alagia, M.; Aquilanti, V.; Ascenzi, D.; Balucani, N.; Cappelletti, D.; Cartechini, L.; Casavecchia, P.; Pirani, F.; Sanchini, G.; Volpi, G. G. *Isr. J. Chem*. **1997**, *37*, 329.
(8) Alagia, M.; Balucani, N.; Cartchini, L.; Casavecchia, P.; Volpi, G. G.; Sato, K.; Takayanagi, T.; Kurosaki, Y. Submitted for publication.
(9) Casavecchia, P. Private communication.
(10) Suzuki, T.; Shihira, Y.; Sato, T.; Umemoto, H.; Tsunashima, S. *J. Chem. Soc., Faraday Trans*. **1993**, *89*, 995.
(11) Takayanagi, T.; Kurosaki, Y.; Misawa, K.; Sugiura, M.; Kobayashi, Y.; Sato, K.; Tsunashima, S. *J. Phys. Chem. A* **1998**, *102*, 6251.
(12) Kobayashi, H.; Takayanagi, T.; Yokoyama, K.; Sato, T.; Tsunashima, S. *J. Chem. Soc., Faraday Trans*. **1995**, *91*, 3771.
(13) Kurosaki, Y.; Takayanagi, T.; Sato, K.; Tsunashima, S. *J. Phys. Chem. A* **1998**, *102*, 254.
(14) Takayanagi, T.; Kurosaki, Y.; Tsunashima, S.; Sato, K. *J. Phys. Chem. A* **1998**, *102*, 10391.
(15) Fell, B.; Rivas, I. V.; McFadden, D. L. *J. Phys. Chem*. **1981**, *85*, 224.
(16) Umemoto, H.; Sugiyama, K.; Tsunashima, S.; Sato, S. *Bull. Chem. Soc. Jpn*. **1985**, *58*, 3076.
(17) Umemoto, H., Hachiya, N.; Matsunaga, E.; Kawasaki, M. *Chem. Phys. Lett*. **1998**, *296*, 203.
(18) Sugawara, K.; Ishikawa, Y.; Sato, S. *Bull. Chem. Soc. Jpn*. **1980**, *53*, 1344.
(19) Sugawara, K.; Ishikawa, Y.; Sato, S. *Bull. Chem. Soc. Jpn*. **1980**, *53*, 3159.
(20) Donovan, R. J.; Husain, D. *Chem. Rev*. **1970**, *70*, 489.
(21) Isaacson, A. D.; Truhlar, D. G.; Rai, S. N.; Steckler, R.; Hancock, G. C.; Garrett, B. C.; Redmon, M. J. *Comput. Phys. Comm*. **1987**, *47*, 91.
(22) Truhlar, D. G. *J. Chem. Phys*. **1972**, *56*, 3189.
(23) Muckerman, J. T.; Newton, M. D. *J. Chem. Phys*. **1972**, *56*, 3191.
(24) Miller, W. H.; Handy, N. C.; Adams, J. E. *J. Chem. Phys*. **1980**, *72*, 99.
(25) Frisch, M. J.; Trucks, G. W.; Schlegel, H. B.; Gill, P. M. W.; Johnson, B. G.; Robb, M. A.; Cheeseman, J. R.; Keith, T.; Petersson, G. A.; Montgomery, J. A.; Raghavachari, K.; Al-Laham, M. A.; Zakrzewski, V. G.; Ortiz, J. V.; Foresman, J. B.; Cioslowski, J.; Stefanov, B. B.; Nanayakkara, A.; Challacombe, M. C.; Peng, Y.; Ayala, P. Y.; Chen, W.; Wong, M. W.; Andres, J. L.; Replogle, E. S.; Gomperts, R.; Martin, R. L.; Fox, D. J.; Binkley, J. S.; Defrees, D. J.; Baker, J.; Stewart, J. P.; Head-Gordon, M.; Gonzalez, C.; Pople, J. A. *Gaussian 94*; Gaussian, Inc.: Pittsburgh, PA, 1995.
(26) Dupuis, M.; Watts, J. D.; Villar, H. O.; Hurst, G. J. B. HONDO, Version 7; *Comput. Phys. Comm*. **1989**, *52*, 415.
(27) Schatz, G. C. *J. Phys. Chem*. **1995**, *99*, 7522.
(28) Clary, D. C.; Dateo, C. E.; Smith, D. *Chem. Phys. Lett*. **1990**, *167*, 1.